Generalized quark transversity distribution of the pion in chiral quark models

Alexander E. Dorokhov,[1,2,*] Wojciech Broniowski,[3,4,†] and Enrique Ruiz Arriola[5,6,‡]

[1]*Joint Institute for Nuclear Research, Bogoliubov Laboratory of Theoretical Physics, 114980, Dubna, Russia*
[2]*Institute for Theoretical Problems of Microphysics, Moscow State University, RU-119899, Moscow, Russia*
[3]*The H. Niewodniczański Institute of Nuclear Physics, Polish Academy of Sciences, PL-31342 Kraków, Poland*
[4]*Institute of Physics, Jan Kochanowski University, PL-25406 Kielce, Poland*
[5]*Departamento de Física Atómica, Molecular y Nuclear, Universidad de Granada, E-18071 Granada, Spain*
[6]*Instituto Carlos I de Fisica Teórica y Computacional, Universidad de Granada, E-18071 Granada, Spain*

(Received 29 July 2011; published 12 October 2011)

The transversity generalized parton distributions (tGPDs) of the pion, involving matrix elements of the tensor bilocal quark current, are analyzed in chiral quark models. We apply the nonlocal chiral models involving a momentum-dependent quark mass, as well as the local Nambu–Jona-Lasinio with the Pauli-Villars regularization to calculate the pion tGPDs, as well as related quantities following from restrained kinematics, evaluation of moments, or taking the Fourier-Bessel transforms to the impact-parameter space. The obtained distributions satisfy the formal requirements, such as proper support and polynomiality, following from Lorentz covariance. We carry out the leading-order QCD evolution from the low quark-model scale to higher lattice scales, applying the method of Kivel and Mankiewicz. We evaluate several lowest-order generalized transversity form factors, accessible from the recent lattice QCD calculations. These form factors, after evolution, agree properly with the lattice data, in support of the fact that the spontaneously broken chiral symmetry is the key element also in the evaluation of the transversity observables.

DOI: 10.1103/PhysRevD.84.074015 PACS numbers: 12.38.Lg, 11.30.Rd, 12.38.−t

I. INTRODUCTION

The underlying spin-$\frac{1}{2}$ partonic structure of hadrons became first manifest in the analysis of the deep inelastic scattering [1]. Actually, further understanding of the partonic spin distributions can be gained by the study of the *transversity distributions* [2]. From this viewpoint, generalized parton distributions (GPDs) [3–5] (for extensive reviews see, e.g., [6–8] and references therein) encode a detailed information on the parton structure of hadrons when analyzed at short distances. In the impact-parameter space, the GPDs can be viewed as partonic probabilities in the infinite-momentum frame distributed along the longitudinal momentum fraction (Bjorken-x) and the transverse space directions [9,10]. It should be noted that both GPDs as well as their partonic interpretation depend strongly on the renormalization scale and it is not obvious *a priori* what, if any, is the reference scale, which might have some universal value and significance. From a dynamical point of view, the choice of such a scale is crucial, as the high-energy modes are integrated out in favor of an effective and yet unknown nonperturbative low-energy dynamics. The renormalization group deals with the intertwining of scales in principle, although in practice it can be explored only at the lowest orders of the perturbation theory in the running strong coupling constant. In addition, GPDs depend also on the factorization scheme corresponding to the physical process used to extract the partonic distributions at high energies.

From a purely theoretical point of view, the great difficulty to determine the GPDs from first principles in QCD is related to their genuine Minkowski-space nature, suggesting application of the light-cone kinematics and nonperturbatively motivated approaches, such as the transverse lattice [11], which so far has produced encouraging but scarce results. More recently, however, the lowest Bjorken-x moments of the kinematically intricate GPDs, the so-called generalized form factors (GFFs), have become directly accessible to Euclidean lattices in QCD at sufficiently short-distance resolution scales (see, e.g., [12,13]). This is due to the fact that GFFs for spacelike momenta can be written as matrix elements of local operators which can be directly extracted from the asymptotics of the Euclidean correlation functions. As a further simplification, the scale dependence of GFFs in the spacelike region undergoes a triangular-matrix multiplicative renormalization, which can be easily implemented (see, e.g., [14]). A well-known feature of the QCD evolution is the loss of resolution at higher energies, a property triggered by the existence of the asymptotic ultraviolet fixed point, which enhances similarity at increasingly high Q^2-values.

In this paper, we analyze the quark *transversity* generalized parton distribution of the pion (tGPD), related to the matrix elements of the bilocal tensor current operator $\bar{q}(x)\sigma_{\mu\nu}q(0)$ (see Sec. II and Refs. [15,16] for precise

*dorokhov@theor.jinr.ru
†Wojciech.Broniowski@ifj.edu.pl
‡earriola@ugr.es

definitions). The transversity distribution, also termed the *maximal helicity* GPD, as it involves aligned parton-helicity operators, provides insight into the nontrivial spin structure of the hadron. For the spin-0 hadrons, tGPDs arise due to a nonzero orbital angular momentum between the initial and final state, and thus offer a unique opportunity to learn about the spin structure without the many complications of the hadronic spin degrees of freedom, as is the case of the nucleon. Because of their inherent complexity, tGPDs are the least investigated among the hadronic GPDs. In this regard, the study of the spin structure of the pion is particularly appealing and challenging, although at present it is unclear how it can be reliably extracted from the high-energy experiments.

The recent lattice determination of the first two X-moments of the pion tGPD, denoted as transversity generalized form factors (tGFFs) [17], provides first important and nontrivial information on this issue. The calculation was carried out at a lattice spacing of $a \sim 0.1$ fm and a pion mass $m_\pi \sim 600$ MeV. For such a small lattice spacing, the matching to the perturbative $\overline{\text{MS}}$ scheme becomes feasible and corresponds to the scale $\mu \simeq 2$ GeV. This lattice calculation has triggered some related studies focusing either on perturbative aspects of the high-Q^2 dependence of the transversity form factors [18], or nonperturbative issues studied within chiral quark models [19,20].

In this work, we analyze the tGPD and the tGFFs of the pion for several chiral quark models, extending the results presented previously [19] and providing further details. While this unavoidably makes the paper a bit technical, we hope that many of the details provided here show how a proper implementation of the chiral symmetry, relativity, and normalization can be achieved in a nonperturbative model calculation. This is particularly interesting for the case of nonlocal models, where the mass function depends on the momentum. Although such models are expected to feature chiral quark dynamics more realistically, many complications arise due to the timelike kinematics implied by the very definition of the GPDs. We recall that we are effectively carrying out the one-loop calculations, where some variables are integrated out and some may be left unintegrated. Thus, special attention must be paid to the treatment of the integrals, particularly to keep the Poincaré invariance explicitly at any step of the calculation, such that all results are mutually consistent.

Via sum rules, the (generalized) form factors are related to the GPDs [6–8,21–26]. Experimentally, the GPDs of the pion constitute rather elusive quantities which appear in rare exclusive processes, such as the deeply virtual Compton scattering or the hard electroproduction of mesons.

Chiral quark models have proved to correctly describe numerous features related to the vector GPD of pion. The parton distribution functions have been evaluated in the Nambu–Jona-Lasinio (NJL) model in Refs. [27–29]. The extension to diagonal GPDs in the impact-parameter space was carried out in [30]. Other analyses of the pionic GPDs and PDFs were performed in nonlocal chiral quark models [31–39], in the NJL model [32,40–43], and in the light-front constituent quark models [44,45]. The parton distribution amplitudes, related to the GPD via a low-energy theorem [46], were evaluated in [47–54]. The gravitational form factors were computed in [55]. Finally, the pion-photon transition distribution amplitudes [56–59] were obtained in Refs. [60–64].

Besides the phenomenological motivation, it is useful to review shortly what aspects of the present investigation suggest the use of chiral quark models within the present context (see, e.g., [54]). Firstly, the pion, treated as a composite $q\bar{q}$ state, becomes a Goldstone boson of the spontaneously broken chiral symmetry. This of course requires the correct implementation of the chiral Ward-Takahashi identities—a rather nontrivial point, since this condition is not automatically fulfilled in loop calculations. At the quark level, this feature is compatible with the large-N_c scaling relations. Within such a scheme, the pion loop corrections are $1/N_c$-suppressed but chiral-log enhanced at small pion masses. However, the leading-N_c contributions present a much milder pion-mass dependence, a favorable situation for the unphysically large pion masses used on the lattice [17]. Moreover, relativity for the GPDs is properly implemented through the so-called polynomiality conditions, and, more specifically, by the explicit use of the double distributions (DDs). Finally, the scale at which a quark model calculation is carried out can only be identified after a correct separation of the momentum fraction carried by the quark degrees of freedom. As mentioned already, the partonic properties depend on the renormalization scale, and according to phenomenology [65,66] as well as independent lattice calculations [67], the (valence) quarks carry about 40% of the total momentum at the scale $\mu = 2$ GeV. In effective quark models, where the quarks carry 100% of the total momentum, the perturbative scale is unexpectedly and rather uncomfortably low. However, the assumption has been tested to higher orders and confronted by comparing to a variety of high-energy data or lattice calculations. In the present calculation of the transversity form factors, we find again agreement with the data after the QCD evolution scheme is implemented, starting from a low quark-model scale.

GPDs in general, and tGPDs in particular, are subjected to a set of conditions *a priori* imposed by symmetries and/or completeness, namely, the chiral symmetry, relativity, positivity, and finiteness of sum rules. Within the framework of low-energy chiral quark models, where there is an inherent cutoff marking the low-energy regime, these conditions are actually not easy to fulfill on purely mathematical grounds. Indeed, one-loop integrals are four

dimensional, whereas GPDs leave two integration variables unintegrated and hence some consistency is required. However, once this difficulty is mastered, which is the case of our approach, there is a trend to independence to details of the model. This independence is largely enhanced *after* the QCD evolution, since differences are washed out at increasingly higher energy scales. The feature is also observed in the study of transversity, as to make differences between various chiral quark models rather small.

We apply the local NJL model with the Pauli-Villars regularization, as well as two variants of the nonlocal chiral quark models inspired by the nontrivial structure of the QCD vacuum [68,69]. These models provide the results at the quark-model scale. After the necessary (multiplicative) QCD evolution [43], our model results are in a quite remarkable agreement with the lattice data for tGFFs. Lower values of the constituent quark mass, ~250 MeV, are preferred.

The outline of the paper is as follows: In Sec. II, we give the general definitions of the pion tGPD and tGFFs. Then we derive these quantities in the nonlocal chiral quark models from the triangle diagram in Sec. III. By using the extremely convenient α-representation, we obtain the corresponding expressions for the tGFFs in the momentum- and impact-parameter spaces, the tGPDs for the isosinglet and isovector channels, and also, in special forward and symmetric kinematics, the distribution of the transversity size of the pion. The analysis is carried out explicitly for specific nonlocal models in Sec. IV. For numerical estimates of these quantities, we use two variants of the chiral nonlocal models and the local NJL model. In Sec. V, we present the QCD evolution of the above quantities in general, as well as show its consequences for the studied models. Numerical results for the transversity distribution functions after evolution are shown in Sec. VI. Finally, in Sec. VII we draw our main conclusions.

II. BASIC DEFINITIONS OF THE TRANSVERSITY FORM FACTORS AND GENERALIZED PARTON DISTRIBUTION

In this section, we provide the basic definitions as well as the kinematics of the transversity observables analyzed in the present work.

The pion u-quark tGFFs, $B^{\pi,u}_{Tni}(t)$, parametrize the matrix element

$$\langle \pi^+(p')|O_T^{\mu\nu\mu_1\cdots\mu_{n-1}}|\pi^+(p)\rangle = \mathcal{T}\mathcal{A}\mathcal{S}\frac{P^\mu q^\nu}{m_\pi}\sum_{\substack{i=0,\\ even}}^{n-1} q^{\mu_1}\ldots q^{\mu_i}P^{\mu_{i+1}}\ldots P^{\mu_{n-1}}B^{\pi,u}_{Tni}(t), \quad (1)$$

where the local tensor quark operator is

$$\mathcal{O}_T^{\mu\nu\mu_1\cdots\mu_{n-1}} = \mathcal{T}\,\mathcal{A}_{(\mu\nu)}\,\mathcal{S}_{(\mu_1\cdots\mu_{N-1})}\,\bar{u}(0)i\sigma^{\mu\nu}i\overleftrightarrow{D}^{\mu_1}\cdots i\overleftrightarrow{D}^{\mu_{n-1}}u(0), \quad (2)$$

with $\overleftrightarrow{D}^\beta = \overleftrightarrow{\partial}^\beta - igA^\beta$ being the QCD covariant derivative, and $\overleftrightarrow{\partial}^\beta = \frac{1}{2}(\overrightarrow{\partial}^\beta - \overleftarrow{\partial}^\beta)$. In Eq. (1), p' and p are the initial and final pion momenta, while $P = \frac{1}{2}(p' + p)$, $q = p' - p$, and $t = -q^2$. The symbol $\mathcal{T}\mathcal{A}\mathcal{S}$ denotes symmetrization ($\mathcal{S}$) in $\nu, \mu_1, \ldots, \mu_{n-1}$, followed by antisymmetrization ($\mathcal{A}$) in μ, ν, with the additional prescription that the traces in all index pairs are subtracted ($\mathcal{T}$). The factor $1/m_\pi$ is introduced by convention in order to have dimensionless form factors [17]. Also, as in [17], we use the positively charged pion and the up-quark density for definiteness.

The above definition, which projects on twist-2 operators, can be implemented in a simple and manifestly covariant way (see, e.g., [18]) by a contraction with two constant auxiliary four-vectors, a and b, satisfying $a^2 = (ab) = 0$ and $b^2 \neq 0$. The tGFFs are then defined via

$$M^{\pi,u}_{Tn}(\xi,t) = \left\langle \pi^+(p') \left| \bar{u}(0)i\sigma^{\mu\nu}a_\mu b_\nu(i\overleftrightarrow{D}_a)^{n-1}u(0) \right| \pi^+(p)\right\rangle = (aP)^{n-1}\frac{[(ap)(bp')]}{m_\pi}\sum_{\substack{i=0,\\ even}}^{n-1}(2\xi)^i B^{\pi,u}_{Tni}(t), \quad (3)$$

where the skewness parameter is defined as[1]

$$\xi = -\frac{(aq)}{2(aP)}, \quad (4)$$

$\xi \in [0, 1]$, and (aq), etc., denote the scalar products of four-vectors. In Eq. (3), $[\ldots]$ denotes the antisymmetrization in a and b.

The tGFFs defined in (3) refer to the u-quarks; those for the d-quarks follow from the isospin symmetry and read

$$B^{\pi,d}_{Tni}(t) = (-1)^n B^{\pi,u}_{Tni}(t). \quad (5)$$

The definition of the corresponding tGPD is [6]

$$\langle \pi^+(p') \mid \bar{u}(-a)i\sigma^{\mu\nu}a_\mu b_\nu u(a) \mid \pi^+(p)\rangle = \frac{[(ap)(bp')]}{m_\pi}\int_{-1}^{1} dX e^{-iX(Pa)}E^{\pi,u}_T(X,\xi,t), \quad (6)$$

where we do not display explicitly the gauge link factor. The tGFFs can be written as the Mellin moments of tGPD of the pion as

$$\int_{-1}^{1} dX X^{n-1}E^{\pi,u}_T(X,\xi,t) = \sum_{\substack{i=0,\\ even}}^{n-1}(2\xi)^i B^{\pi,u}_{Tni}(t). \quad (7)$$

[1]Throughout this work we use the so-called symmetric notation.

III. CHIRAL QUARK MODELS

In this section, we review the generic one-loop features of chiral quark models, where the quark self-energy as well as the interaction vertices are assumed to have a fairly general momentum dependence to be specified later on. We derive general expressions for the tGPD at the one-quark-loop level, applicable to both nonlocal and local models. We also display formal properties of tGPD in our approach.

A. Nonlocal chiral quark models

In the quark-model calculation in the large-N_c limit, the matrix element (3) is given by the triangle diagram shown in Fig. 1.[2] To calculate this diagram, we explore the manifestly covariant method based on the effective approach to nonperturbative QCD dynamics. All expressions will be computed in the Euclidean space, appropriate for the process under consideration and, in general, for the treatment of nonperturbative physics. The nonperturbative quark propagator, dressed by the interaction with the QCD vacuum, is assumed to have the form

$$S(k) = \frac{\hat{k} + m(k^2)}{D(k^2)}. \tag{8}$$

The main requirement imposed on the quark propagator is that at large quark virtualities one recovers the perturbative limit,

$$S(k) \overset{k^2\to\infty}{\to} \frac{\hat{k}}{k^2}. \tag{9}$$

It is also assumed that the dynamical quark mass, $m(k^2)$, is a function rapidly dropping with the quark virtuality k^2. It is normalized at zero as

$$m(0) = M_q, \qquad D(0) = M_q^2. \tag{10}$$

We also need the quark-pion vertex[3]

$$\Gamma_\pi^a(k, q) = \frac{i}{f_\pi}\gamma_5\tau^a F(k_+^2, k_-^2), \tag{11}$$

where $k_\pm = k \pm q/2$. The nonlocal vertex $F(k_+^2, k_-^2)$ is a symmetric function of its arguments, normalized to $F(k^2, k^2) = m(k^2)$. In the present study, the nonlocal model calculations are performed in the strict chiral limit, which means that $m(k^2 \to \infty) = 0$.

[2]We should emphasize at this point that the tensor matrix element (3) cannot be induced by tadpole-type diagrams. This is evident, because these diagrams depend only on one external vector q from which it is impossible to construct the antisymmetric combination involving the matrix element (3). In this aspect, the results obtained in [20] cannot be correct.

[3]In this work, we use the dominant (in the spontaneous symmetry-breaking mechanism) structures for the quark propagator and the quark-pion vertex. More general structures are used in the Schwinger-Dyson approach [70].

B. Calculation of the triangle diagram

Within the described approach, the triangle diagram for the matrix element (3) yields

$$M_{Tn}(\xi, t) = \frac{N_c}{4\pi^2 f_\pi^2}\int\frac{d^4k}{\pi^2}F(k_+^2, k_-^2)F(k_3^2, k_-^2) \times \frac{1}{4}\,\mathrm{Tr}\{S(k_+)\gamma_5 S(k_-)\gamma_5 S(k_3)\sigma_{\mu\nu}\} \times \left(\frac{k_+ + k_3}{2}, a\right)^{n-1} a_\mu b_\nu, \tag{12}$$

where $k_+ = k$ is the initial momentum of the struck quark, $k_3 = k_+ + q$ is its final momentum, $k_- = k_+ - p$ is the momentum of the spectator quark (cf. Fig. 1), and the covariant average momentum $(k_+ + k_3)/2$ corresponds to the derivative in the definition (3).

After taking the trace, one has

$$M_{Tn}(\xi, t) = \frac{N_c}{4\pi^2 f_\pi^2}\int\frac{d^4k}{\pi^2}\frac{F(k_+^2, k_-^2)F(k_3^2, k_-^2)}{D(k_+^2)D(k_-^2)D(k_3^2)} \times \{m(k_+^2)[(k_- a)(k_3 b)] - m(k_-^2)[(k_+ a)(k_3 b)] + m(k_3^2)[(k_+ a)(k_- b)]\}\left(\frac{k_+ + k_3}{2}, a\right)^{n-1}, \tag{13}$$

where the antisymmetrization in a and b is implied. Considering the crossed channel, it is easy to get the relation

$$\left(\{\ldots\}\left(\frac{k_+ + k_3}{2}, a\right)^{n-1}\right)_{d-\text{channel}} \to (-1)^n\left(\{\ldots\}\left(\frac{k_+ + k_3}{2}, a\right)^{n-1}\right)_{u-\text{channel}}, \tag{14}$$

in agreement with (5).

For the further analysis, it is very convenient to transform the integral in (13) into the α-representation (see [71,72]), which is one of the basic methods for the study of hard processes in perturbative QCD [73], as well as in nonperturbative quark models [33]. The technical advantage of this method is the explicit maintenance of the Lorentz covariance.

Let us define for any function F of virtuality k^2, decaying at large virtuality as $1/k^2$ or faster, its α representation (Laplace transform)

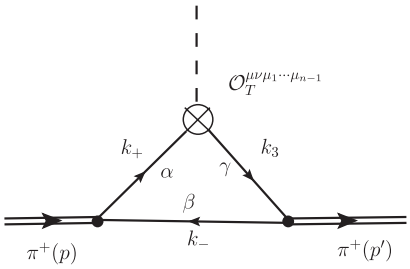

FIG. 1. (Color online) The leading-N_c one-quark-loop triangle diagram contribution to the leading twist tGPD of the pion.

$$F(k^2) = \int_0^\infty d\alpha e^{-\alpha k^2} f(\alpha) \tag{15}$$

where $F(k^2)$ is the image of the original function $f(\alpha)$. We will use the shorthand $F(k^2) \sim f(\alpha)$. Let us introduce the following notation: [74,75]

$$\begin{aligned}
&\frac{F(k_+^2, k_-^2)F(k_3^2, k_-^2)}{D(k_+^2)D(k_-^2)D(k_3^2)} m(k_+^2) \sim G_{m,0,0}(\alpha, \beta, \gamma),\\
&\frac{F(k_+^2, k_-^2)F(k_3^2, k_-^2)}{D(k_+^2)D(k_-^2)D(k_3^2)} m(k_-^2) \sim G_{0,m,0}(\alpha, \beta, \gamma),\\
&\frac{F(k_+^2, k_-^2)F(k_3^2, k_-^2)}{D(k_+^2)D(k_-^2)D(k_3^2)} m(k_3^2) \sim G_{0,0,m}(\alpha, \beta, \gamma),
\end{aligned} \tag{16}$$

where the triple α representation (i.e., in parameters α, β, and γ) is applied (see Fig. 1). With this notation, the momentum integral in Eq. (13) is transformed into the α-representation expression for the matrix element,

$$\begin{aligned}
M_{Tn}(\xi, t) = (aP)^{n-1}[(ap)(bp')]\frac{N_c}{4\pi^2 f_\pi^2}
&\times \int \frac{d(\alpha\beta\gamma)}{\Delta^3} e^{-(1/\Delta)(\alpha\gamma t - \beta(\alpha+\gamma)m_\pi^2)}\\
&\times \left(\frac{\beta + (\gamma - \alpha)\xi}{\Delta}\right)^{n-1} [\alpha G_{m,0,0}(\alpha, \beta, \gamma)\\
&+ \beta G_{0,m,0}(\alpha, \beta, \gamma) + \gamma G_{0,0,m}(\alpha, \beta, \gamma)],
\end{aligned} \tag{17}$$

where $\Delta = \alpha + \beta + \gamma$ and

$$\int d(\alpha\beta\gamma)\ldots = \int_0^\infty d\alpha \int_0^\infty d\beta \int_0^\infty d\gamma \ldots \tag{18}$$

The only dependence on ξ in Eq. (17) appears in the polynomial factor in the third line. It is clear that in the expansion of this polynomial in powers of ξ only the even powers survive, in accordance with Eq. (3), since for the odd powers of ξ the integrand is antisymmetric in α and γ. Thus the polynomiality property of Eq. (7), namely, that the X^{n-1} moment of $E_T^\pi(X, \xi, t)$ is a polynomial in ξ of the order not higher than n, is immediately evident within our approach.

C. Transversity pion form factors in momentum and impact-parameter spaces

From representation (17), by using the definition of the tGFFs (3), one gets[4]

$$\begin{aligned}
B_{Tni}^u(t) = \frac{N_c}{4\pi^2 f_\pi^2} \frac{(n-1)!}{i!(n-1-i)!}
&\times \int \frac{d(\alpha\beta\gamma)}{\Delta^{n+2}} e^{-(\alpha\gamma/\Delta)t} [2\alpha G_{m,0,0}(\alpha, \beta, \gamma)\\
&+ \beta G_{0,m,0}(\alpha, \beta, \gamma)]\beta^{n-1-i}\left(\frac{\gamma - \alpha}{2}\right)^i,
\end{aligned} \tag{19}$$

where $i = 0, 2, \ldots \le n-1$, and the symmetry properties under the interchange of α and γ has been used. The transverse (impact parameter) space representation is obtained, by definition, after a 2D Fourier-Bessel transformation,

$$F(b_\perp^2) = \int \frac{d^2 q_\perp}{(2\pi)^2} e^{-i(b_\perp q_\perp)} F(t = -q_\perp^2). \tag{20}$$

We then get for even i the expression

$$\begin{aligned}
B_{Tni}^u(b_\perp^2) = \frac{N_c}{16\pi^3 f_\pi^2} \frac{(n-1)!}{i!(n-1-i)!}
&\times \int \frac{d(\alpha\beta\gamma)}{\alpha\gamma\Delta^{n+1}} e^{-(\Delta/\alpha\gamma)(b_\perp^2/4)} [2\alpha G_{m,0,0}(\alpha, \beta, \gamma)\\
&+ \beta G_{0,m,0}(\alpha, \beta, \gamma)]\beta^{n-1-i}\left(\frac{\gamma - \alpha}{2}\right)^i.
\end{aligned} \tag{21}$$

D. Pion transversity generalized parton distribution

Through the use of the definition of the tGPD in Eq. (7), we arrive at the formula

$$\begin{aligned}
E_T^\pi(X, \xi, t) = \frac{N_c}{4\pi^2 f_\pi^2}
&\times \int \frac{d(\alpha\beta\gamma)}{\Delta^3} e^{-(\alpha\gamma/\Delta)t} [\alpha G_{m,0,0}(\alpha, \beta, \gamma)\\
&+ \beta G_{0,m,0}(\alpha, \beta, \gamma) + \gamma G_{0,0,m}(\alpha, \beta, \gamma)]\\
&\times \delta\left(X - \frac{\beta + (\gamma - \alpha)\xi}{\Delta}\right),\\
&-1 < X = \frac{\beta + (\gamma - \alpha)\xi}{\Delta} < 1.
\end{aligned} \tag{22}$$

Let us integrate over the β parameter, corresponding to the quark spectator. From the δ function, we resolve β as

$$\beta = \frac{(X + \xi)\alpha + (X - \xi)\gamma}{1 - X} \tag{23}$$

and apply the positivity conditions for α, β, and γ. At fixed $\xi \in [0, 1]$ and $X \in [-1, 1]$, one has three distinct regions:

I. $\xi < X < 1$, where $X + \xi > 0$, $X - \xi > 0$,

II. $-\xi < X < \xi$, where $X + \xi > 0$, $X - \xi < 0$,

III. $-1 < X < -\xi$, where $X + \xi < 0$, $X - \xi < 0$.

[4] In the following, we will explore the strict chiral limit of $m_\pi = 0$.

In region I, β is positive without any limitations. In region III, all coefficients in Eq. (23) are negative, hence the support of the integrand has zero measure and the integral in Eq. (22) equals zero. In the central region II, the coefficient of α in Eq. (23) is positive and the coefficient of γ is negative, thus one has the limitation $\alpha > \gamma\frac{\xi-X}{\xi+X}$. Finally, the total result may be combined as

$$E_T^\pi(X,\xi,t) = \Theta(X+\xi)\frac{N_c}{4\pi^2 f_\pi^2}\int_0^\infty d\gamma \int_{\max\{0,\gamma\frac{\xi-X}{\xi+X}\}}^\infty d\alpha e^{-(\alpha\gamma/\Delta)t}\frac{\alpha G_{m,0,0}(\alpha,\beta,\gamma)+\beta G_{0,m,0}(\alpha,\beta,\gamma)+\gamma G_{0,0,m}(\alpha,\beta,\gamma)}{\Delta^2(1-X)}, \tag{24}$$

where $\Theta(x)$ is the step function, β is given by Eq. (23), and $\Delta = [\alpha+\gamma+\xi(\alpha-\gamma)]/(1-X)$.

The isovector and isosinglet tGPDs of the pion are obtained as the symmetric and antisymmetric combinations,

$$\begin{aligned} E_T^{\pi,I=1}(X,\xi,Q^2) &\equiv E_T^{\pi,S}(X,\xi,Q^2) \\ &= E_T^\pi(X,\xi,Q^2) + E_T^\pi(-X,\xi,Q^2), \\ E_T^{\pi,I=0}(X,\xi,Q^2) &\equiv E_T^{\pi,A}(X,\xi,Q^2) \\ &= E_T^\pi(X,\xi,Q^2) - E_T^\pi(-X,\xi,Q^2). \end{aligned} \tag{25}$$

The support of $E_T^{\pi,I=0,1}$ is $-1 \le X \le 1$. The significance of the isospin combinations comes from the fact that they evolve autonomously with the renormalization scale, see Sec. V.

E. Special kinematics: $\xi = 0$ and $\xi = X$ cases

Some special kinematics is evident. For the case $\xi = 0$ (tPDF), we have

$$\begin{aligned} E_T^\pi(X,\xi=0,t) &= \Theta(X)\frac{N_c}{4\pi^2 f_\pi^2}\int_0^\infty d(\alpha\gamma)e^{-(\alpha\gamma/\Delta)t} \\ &\times \frac{2\alpha G_{m,0,0}(\alpha,\beta,\gamma)+\beta G_{0,m,0}(\alpha,\beta,\gamma)}{\Delta^2(1-X)}, \end{aligned} \tag{26}$$

where $\beta = (\alpha+\gamma)\frac{X}{1-X}$ and $\Delta = (\alpha+\gamma)\frac{1}{1-X}$. Note that in general the first term in the numerator dominates in the small X region, while the second one is more important in the region of large X.

For the border case, $\xi = X$, we find

$$E_T^\pi(X,\xi=X,t) = \Theta(X)\frac{N_c}{4\pi^2 f_\pi^2}\int_0^\infty d(\alpha\gamma)e^{-(\alpha\gamma/\Delta)t}\frac{\alpha G_{m,0,0}(\alpha,\beta,\gamma)+\beta G_{0,m,0}(\alpha,\beta,\gamma)+\gamma G_{0,0,m}(\alpha,\beta,\gamma)}{\Delta^2(1-X)}, \tag{27}$$

with $\beta = 2\alpha\frac{X}{1-X}$ and $\Delta = [\alpha+\gamma+X(\alpha-\gamma)]\frac{1}{1-X}$.

F. Double distribution

Some symmetry properties of the GPDs are more transparent when they are constructed from the DDs [3,5,76]. Actually, the relativistic invariance exhibited by the polynomiality conditions is manifestly built-in in this approach (see, e.g., Ref. [77]). To pass to double distributions, we first make the substitution (see, e.g., [76]) $\alpha = x_1 L$, $\beta = x_2 L$, $\gamma = x_3 L$ in Eq. (22) and obtain

$$\begin{aligned} E_T^\pi(X,\xi,t) = \frac{N_c}{4\pi^2 f_\pi^2}\int_0^\infty dL \int_0^1 dx_1 dx_2 dx_3 e^{-x_1 x_3 t} \\ \times \delta(1-x_1-x_2-x_3) \\ \times \delta(x-x_2-(x_3-x_1)\xi) \\ \times [x_1 G_{m,0,0}(x_1 L, x_2 L, x_3 L) \\ + x_2 G_{0,m,0}(x_1 L, x_2 L, x_3 L) \\ + x_3 G_{0,0,m}(x_1 L, x_2 L, x_3 L)]. \end{aligned} \tag{28}$$

To recover the DD representation we further make the replacement $x_2 = b$, $x_3 - x_1 = a$ and arrive at

$$E_T^\pi(X,\xi,t) = \int_0^1 db \int_{-1+b}^{1-b} da\,\delta(X-b-a\xi) f_T^\pi(a,b,t), \tag{29}$$

with the DD identified as

$$\begin{aligned} f_T^\pi(a,b,t) = \frac{N_c}{4\pi^2 f_\pi^2}\int_0^\infty dL e^{-x_1 x_3 t} \\ \times [x_1 G_{m,0,0}(x_1 L, bL, x_3 L) \\ + bG_{0,m,0}(x_1 L, bL, x_3 L) \\ + x_3 G_{0,0,m}(x_1 L, bL, x_3 L)]. \end{aligned} \tag{30}$$

Here, $x_1 = \frac{1}{2}(1-b-a)$ and $x_3 = \frac{1}{2}(1-b+a)$. In the above expressions, the parameter b is non-negative. The $b \le 0$ part of the DD comes from the crossed diagram.

Sometimes it is also convenient to separate the so-called D-term, defined as

$$D(b,t) = \int_{-1+b}^{1-b} da f_T^\pi(a,b,t). \tag{31}$$

G. The $b_\perp$ space and the transverse pion size

Let us now consider tGPD in the transverse coordinate space, $b_\perp$. By using the 2D Fourier-Bessel transform of Eq. (20), one easily gets

$$E_T^\pi(X,\xi,b_\perp^2) = \Theta(X+\xi)\frac{N_c}{16\pi^3 f_\pi^2}\int_0^\infty d\gamma \int_{\max\{0,\gamma(\xi-X/\xi+X)\}}^\infty d\alpha e^{-(\Delta/\alpha\gamma)(b_\perp^2/4)} \times \frac{\alpha G_{m,0,0}(\alpha,\beta,\gamma)+\beta G_{0,m,0}(\alpha,\beta,\gamma)+\gamma G_{0,0,m}(\alpha,\beta,\gamma)}{\Delta\alpha\gamma(1-X)}, \tag{32}$$

where the value of the parameter β is given by Eq. (23) and $\Delta = [\alpha+\gamma+\xi(\alpha-\gamma)]\frac{1}{1-X}$.

In the zero longitudinal momentum-transfer limit, $\xi \to 0$, one obtains the so-called 3D transverse parton distribution

$$f_T^\pi(X, b_\perp) = E_T^\pi(X, \xi \to 0, b_\perp^2). \tag{33}$$

Following [78], one can also introduce the normalized quark probability density in the transverse plane,

$$\rho_T^\pi(X, b_\perp) = \frac{f_T^\pi(X, b_\perp)}{f_T^\pi(X)}, \tag{34}$$

where

$$f_T^\pi(X) \equiv E_T^\pi(X, \xi = 0, t = 0), \tag{35}$$

as defined in (26). The partons with the longitudinal momentum fraction X occupy within the hadron a disc of the average transverse radius squared given by

$$b_\perp^2(X) = \int d^2b_\perp b_\perp^2 f_T^\pi(X, b_\perp). \tag{36}$$

In chiral quark models, the triangle diagram yields

$$b_\perp^2(X) = \frac{N_c}{\pi^2 f_\pi^2}(1-X)^2\int d(\alpha\gamma)\frac{\alpha\gamma}{(\alpha+\gamma)^3} \times [2\alpha G_{m,0,0}(\alpha,\beta,\gamma)+\beta G_{0,m,0}(\alpha,\beta,\gamma)], \tag{37}$$

where $\beta = (\alpha+\gamma)\frac{X}{1-X}$. The C-odd transverse size of the hadron, determined by the slope of the tGFF at low momentum transfer, can be obtained by integrating $b_\perp^2(X)$ over the momentum fraction

$$b_\perp^2 = 2\int_0^1 dX b_\perp^2(X). \tag{38}$$

According to Gribov [79], one can interpret the normalized quark density (34) as an evolution of the probability density for a stochastic motion of a particle in the transverse plane. The role of the evolution time is played by the rapidity variable, $\eta = \ln(1/X)$. For the stochastic process, one can introduce the mean squared distance of the particle as follows: [78]:

$$d_\perp^2(X) = \int d^2b_\perp b_\perp^2 \rho(X, b_\perp) = \frac{b_\perp^2(X)}{f(X)}. \tag{39}$$

By using a model with short-range interactions, Gribov predicted that [79]

$$d_\perp^2(\eta) = D\eta, \tag{40}$$

where D is a constant, while in [78] the result is

$$d_\perp^2(\eta) \sim \frac{1}{(4\pi f_\pi)^2}e^{(1-\omega)\eta}. \tag{41}$$

Here, $\omega \approx 0.5$ is the slope of the forward quark distribution at small X, i.e., $q(X) \sim 1/X^\omega$. Note that Eq. (41) is $\mathcal{O}(N_c^{-1})$, since $f_\pi = \mathcal{O}(\sqrt{N_c})$. Actually, the "chiral inflation" discussed in Ref. [78] is a pion-loop effect, which is $1/N_c$-suppressed, but at the same time it is chirally enhanced as $\log(m_\pi^2)$ for $m_\pi \to 0$, compared to the leading one-quark-loop contribution. In the real world with $N_c = 3$ and $m_\pi = 140$ MeV, the relative chiral contributions to the rms radius of the pion are about 20% [80]. [5] Of course, the additional inclusion of pion-loops in our model would automatically reproduce this universal inflating phenomenon.

IV. MODEL RESULTS

Having derived the general formulas for tGPDs in chiral quark models from the triangle diagram of Fig. 1, we now pass to presenting explicit numerical calculations. We start with the nonlocal models. In the present work, we consider two variants of the quark-pion vertex of Eq. (11),

$$F_{\rm I}(k_+^2, k_-^2) = \sqrt{m(k_+^2)m(k_-^2)}, \tag{42}$$

$$F_{\rm HTV}(k_+^2, k_-^2) = \frac{1}{2}[m(k_+^2)+m(k_-^2)], \tag{43}$$

where $m(k^2)$ is the momentum-dependent dynamical quark mass. The form (42) is motivated by the instanton picture of the QCD vacuum [68] and is labeled "instanton," while the form (43), the Holdom-Terning-Verbeek (HTV) vertex, comes from the nonlocal chiral quark model of Ref. [69].

[5] Actually, from the relation for the rms radius of the pion found in ChPT [80], $\langle r^2\rangle = (\bar{l}_5 - 1)/(16\pi^2 f_\pi^2)$, one has the *total* low-energy constant $\bar{l}_5 = 13.9 \pm 1.3$, most of which is saturated by the ρ-meson exchange, $\bar{l}_5^\rho \simeq 17$, at the leading order in N_c. Thus, the subleading ($1/N_c$-suppressed) contribution is estimated to be $\Delta\bar{l}_5 \equiv \bar{l}_5 - \bar{l}_5^\rho \sim \log(m_\pi^2/m_\rho^2) \sim -3$.

Some relevant differences between both prescriptions regarding the proper implementation of chiral symmetry are discussed in Ref. [81].

We consider the dynamical quark mass of the form

$$m(k^2) = M_q f^2(k^2), \tag{44}$$

and for simplicity take the profile function $f(k^2)$ as a Gaussian,

$$f(k^2) = e^{-\Lambda k^2} \tag{45}$$

(note that Λ has the interpretation of the squared inverse momentum cutoff). The model contains two parameters: the dynamical quark mass at zero momentum, M_q, and the nonlocality scale, Λ. For our numerical estimates we take one parameter fixed at a physically reasonable value, $M_q \simeq 240$ MeV, and then fix Λ via the pion decay constant evaluated in the chiral limit, $f_\pi = 84$ MeV [80]. The expression for f_π in the instanton model is given by the Diakonov-Petrov formula [68],

$$f_\pi^{\mathrm{I}} = \left[\frac{N_c}{4\pi^2}\int_0^\infty du u \frac{m(u)}{D^2(u)}(m(u) - um'(u) + u^2 m'^2(u))\right]^{1/2}, \tag{46}$$

while in the HTV model one has the Pagels-Stokar formula [69,82]

$$f_\pi^{\mathrm{HTV}} = \left[\frac{N_c}{4\pi^2}\int_0^\infty du u \frac{m(u)}{D^2(u)}\left(m(u) - \frac{1}{2}um'(u)\right)\right]^{1/2}. \tag{47}$$

The described parameter-fitting procedure yields

$$\Lambda_{\mathrm{I}} = 0.7\ \mathrm{GeV}^{-2}, \qquad \Lambda_{\mathrm{HTV}} = 0.375\ \mathrm{GeV}^{-2}. \tag{48}$$

For the instanton model, the integrand in Eq. (17) and the subsequent formulas can be expressed as follows:

$$\alpha G_{m,0,0}(\alpha,\beta,\gamma) + \beta G_{0,m,0}(\alpha,\beta,\gamma) + \gamma G_{0,0,m}(\alpha,\beta,\gamma) \xrightarrow{\mathrm{I}} \alpha d_\alpha^{3/2} d_\beta^1 d_\gamma^{1/2} + \beta d_\alpha^{1/2} d_\beta^2 d_\gamma^{1/2} + \gamma d_\alpha^{1/2} d_\beta^1 d_\gamma^{3/2}, \tag{49}$$

while for the HTV model one has

$$\begin{aligned}\alpha G_{m,0,0}(\alpha,\beta,\gamma) + \beta G_{0,m,0}(\alpha,\beta,\gamma) + \gamma G_{0,0,m}(\alpha,\beta,\gamma) \xrightarrow{\mathrm{HTV}} \frac{1}{4}\{&\alpha(d_\alpha^2 d_\beta^1 d_\gamma^0 + d_\alpha^2 d_\beta^0 d_\gamma^1 + d_\alpha^1 d_\beta^2 d_\gamma^0 + d_\alpha^1 d_\beta^1 d_\gamma^1) \\ &+ (\alpha \leftrightarrow \gamma) + \beta(d_\alpha^1 d_\beta^2 d_\gamma^0 + d_\alpha^0 d_\beta^2 d_\gamma^1 + d_\alpha^0 d_\beta^3 d_\gamma^0 \\ &+ d_\alpha^1 d_\beta^1 d_\gamma^1).\end{aligned} \tag{50}$$

Here we have introduced the shorthand notation

$$\frac{m^{2n}(k^2)}{D(k^2)} \sim d_\alpha^n. \tag{51}$$

For the assumed Gaussian form factor (45), the d_α^n function at large $\alpha \gg \Lambda$ has the following behavior:

$$\frac{1}{R(\lambda)} M_q^n e^{-\lambda(\alpha - 2n\Lambda)}\Theta(\alpha - 2n\Lambda), \tag{52}$$

with

$$R(\lambda) = 1 - 4\Lambda m^2(\lambda), \tag{53}$$

where λ is the root of the equation

$$\lambda + m^2(\lambda) = 0. \tag{54}$$

The functions (52) can also be used as approximants for the analytic calculations of the quark distributions in the pion. In the momentum representation, this simplification means that in the denominators of the integrands we neglect the momentum dependence of the dynamical quark mass, as would be the case of the local quark models.

A. The numerical results for nonlocal models

In this subsection, we present the results for the nonlocal models. These results are obtained from the formulas presented above with the help of numerical integration.

We start by exploring the t-dependence. In Fig. 2, we present the pion u-quark tGFFs in the HTV model and in the instanton model. First of all, the increase of the indices n or i causes a decrease of the form factor normalization. We also note a faster falloff with t of the tGFFs for the case of the instanton model compared to the HTV case. We note that the tGFFs undergo the QCD evolution, which will be discussed in detail in Sec. V. The $B_{n0}^{\pi,u}$ form factors, however, evolve multiplicatively, hence we can read off their t-dependence from Fig. 2.

At large t, the $B_{10}^{\pi,u}$ form factor in the HTV model has the asymptotic behavior $\sim \ln t/t$. This follows from the asymptotic formula

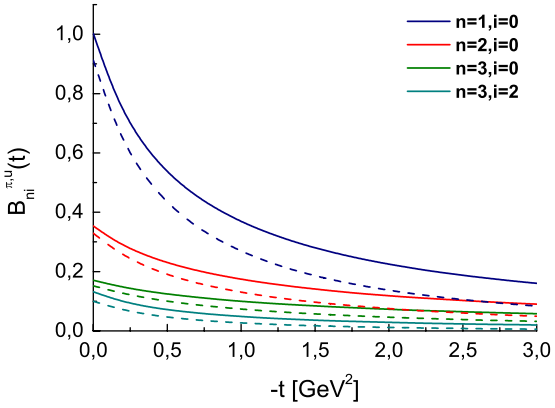

FIG. 2 (color online). (Color online) The tGFFs $B_{ni}^{\pi,u}(t)$ in the HTV model (solid line) and in the instanton model (dashed line) for several lowest values of n and i. The sequence in the legend corresponds to the sequence of the curves, from top to bottom.

$$B^u_{T10}(t \gg \Lambda^{-1}) \overset{\text{HTV}}{=} \frac{1}{t}\frac{N_c}{16\pi^2 f_\pi^2}\Big[\int_0^\infty du \frac{m^3(u)}{D(u)} \ln\Big(\frac{t}{u}\Big) + 2\int_0^\infty du \frac{m^2(u)}{D(u)} \int_0^\infty dv \frac{m(u+v)}{D(u+v)} \times \Big(1 - \frac{m(u)m(u+v)}{u+v}\Big)\Big]. \quad (55)$$

For the instanton model, the falloff is exponential, since

$$B^u_{T10}(t \gg \Lambda^{-1}) \overset{\text{I}}{=} \frac{N_c}{4\pi^2 f_\pi^2}\frac{\sqrt{\pi}M_q^3}{R(\lambda)}\frac{1}{t}\frac{1}{\sqrt{\Lambda\sqrt{\lambda t}}} \times \Big(1 - 2\sqrt{\frac{\lambda}{t}}\Big) e^{-\Lambda(\sqrt{\lambda t} - 6\lambda)} E_1(\Lambda\sqrt{\lambda t}). \quad (56)$$

In Fig. 3, we display the tGFFs in the impact-parameter space. The information is the same as in Fig. 2, as the two figures are simply linked with a Fourier-Bessel transform. Nevertheless, the different large-t behavior of the instanton and HTV models is very vividly seen in the small-b_T behavior in Fig. 3.

Next, we explore the X dependence in the simplest case of $t = 0$ and $\xi = 0$ (tPDF). In Fig. 4, we present the results of calculations of the tPDF in the nonlocal models (35). We notice a more-less triangular shape for both models, with a depletion near $X = 0$.

The end point behavior of these functions can be inferred from Eq. (26) by using the approximants (52). The $X \to 1$ behavior is governed by the properties of the active dynamical quark, while the $X \to 0$ behavior is related to the spectator quark. For the instanton model the end point behavior is exponentially suppressed, namely

$$f_T^I(X \to 1) \sim (1-X)^2 \exp\Big[-\frac{2\lambda\Lambda}{1-X}\Big], \qquad f_T^I(X \to 0) \sim \exp\Big[-\frac{2\lambda\Lambda}{X}\Big], \quad (57)$$

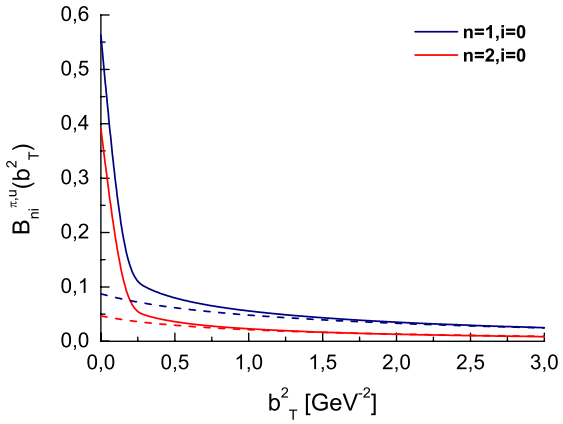

FIG. 3 (color online). (Color online) The tGFFs $B^{\pi,u}_{ni}(b_T^2)$ in the impact parameter space in the HTV model (solid line) and in the instanton model (dashed line). The sequence in the legend corresponds to the sequence of the curves, from top to bottom.

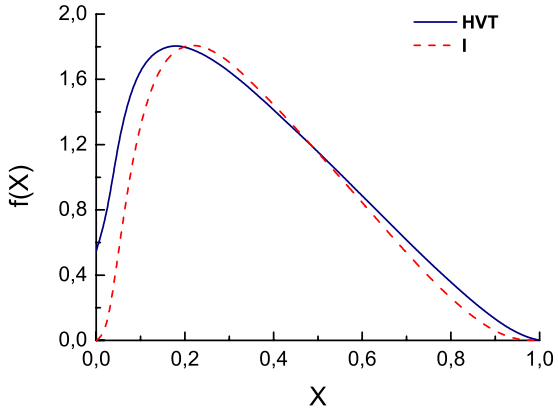

FIG. 4 (color online). (Color online) The tPDF in the HTV model (solid line) and in the instanton model (dashed line).

while for the HVT model one has a powerlike behavior

$$f_T^{\text{HVT}}(X \to 1) \sim (1-X), \qquad f_T^{\text{HVT}}(X \to 0) \sim \text{const}. \quad (58)$$

We remark here that the end point behavior in Eqs. (57) and (58) is sensitive to the radiative corrections, hence it evolves with the scale.

A similar behavior is obtained for the transverse size distribution at $t = 0$, shown in Fig. 5, namely

$$b^2_{\perp I}(X \to 1) \sim (1-X)^4 \exp\Big[-\frac{2\lambda\Lambda}{1-X}\Big], \qquad b^2_{\perp I}(X \to 0) \sim \frac{1}{X}\exp\Big[-\frac{2\lambda\Lambda}{X}\Big], \qquad b^2_{\perp \text{HVT}}(X \to 1) \sim (1-X)^3, \qquad b^2_{\perp \text{HVT}}(X \to 0) \sim \text{const}. \quad (59)$$

Next, we present our results for the distribution function of the mean square distance. In Fig. 6, we show $d_\perp^2$ as a function of X, while in Fig. 7 we present the same quantity as a function of the rapidity variable η. We also compare

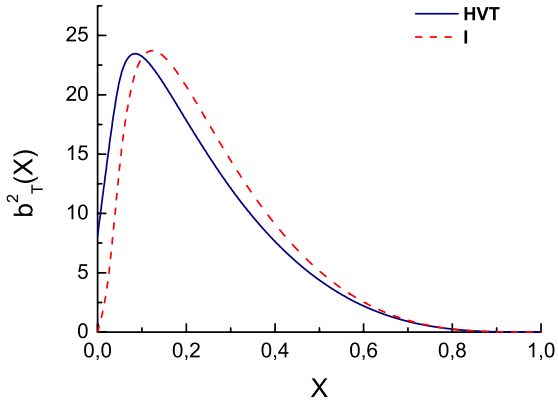

FIG. 5 (color online). (Color online) The distribution function of the transverse size in the HTV model (solid line) and in the instanton model (dashed line).

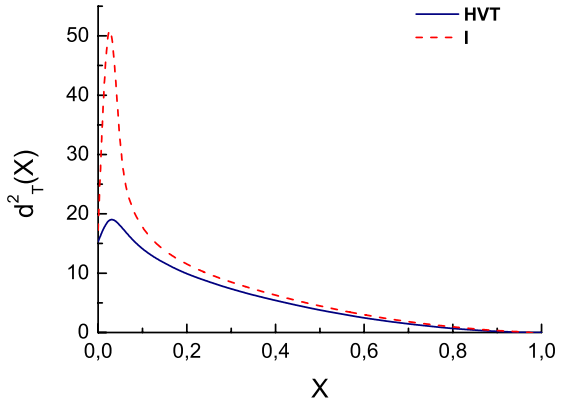

FIG. 6 (color online). (Color online) The distribution function of the mean square distance in the HTV model (solid line) and in the instanton model (dashed line), plotted as a function of X.

our results to the calculations of Refs. [79] (G) and [78] (PPV). In the region of large η, corresponding to low X, various model predictions are different.

Finally, we explore the dependence on ξ and X of the pion tGPDs at $t = 0$. The results are given in Figs. 8 and 9. We note the symmetry properties following from the definition (25). We can also see that the curves bend near $X = \xi$.

To summarize the study of this subsection we state that the results, apart for mathematically different end point behavior, are qualitatively similar in the two explored variants of the nonlocal chiral quark models.

B. Nambu–Jona-Lasinio model

We term the usual Nambu–Jona-Lasinio model with pointlike quark-quark interactions the *local* NJL model. All formulas for the local model follow from the nonlocal expressions given above, with the constant quark mass,

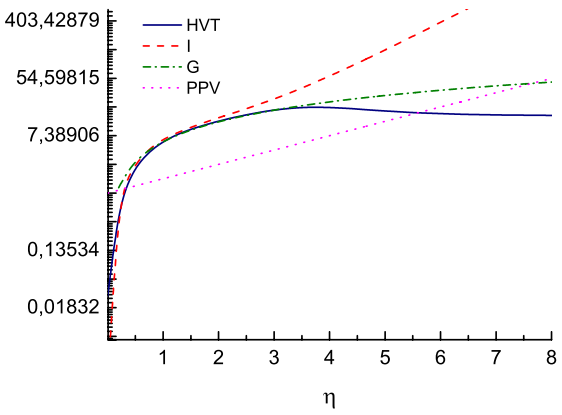

FIG. 7 (color online). (Color online) The distribution function of the mean square distance as function of rapidity η in the HTV model (solid line), in the instanton model (dashed line), in the Gribov approach [79] (G) (dot-dashed line), and in the PPV model [78] (dotted line).

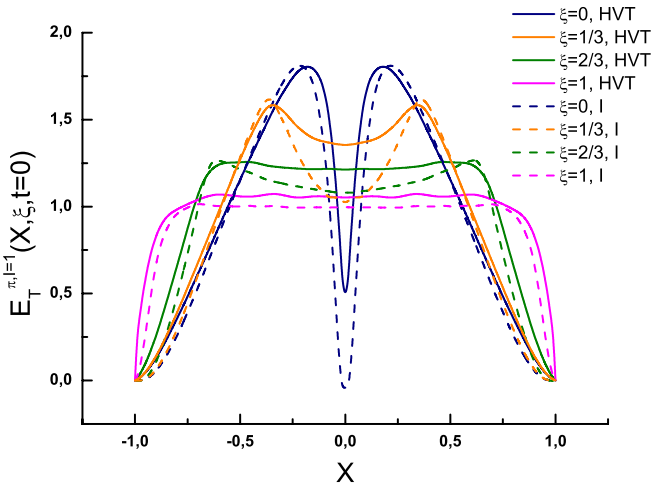

FIG. 8 (color online). (Color online) The pion tGPD for isovector case in the HTV model (solid lines) and in the instanton model (dashed lines) for several values of ξ.

which formally corresponds to taking the limit $\Lambda \to 0$. In addition, a regularization prescription, necessary to make the divergent integrals finite, is implemented, as discussed below.

The one-quark-loop action of the NJL model is

$$\Gamma_{\mathrm{NJL}} = -iN_c \,\mathrm{Tr}\log(i\partial\!\!\!/ - MU^5 - m)|_{\mathrm{reg}}, \qquad (60)$$

where M is the constituent quark mass generated via the spontaneous breaking of the chiral symmetry,

$$U^5 = \exp(i\gamma_5 \boldsymbol{\phi}\cdot\boldsymbol{\tau}), \qquad (61)$$

with $\boldsymbol{\phi}$ denoting the pion field, while m is the current quark mass. We apply the NJL with the Pauli-Villars regularization in the twice-subtracted version of Refs. [54,83,84]. Variants of chiral quark models differ in the way of performing the necessary regularization of the quark loop diagrams, which may to some extent influence the physical results.

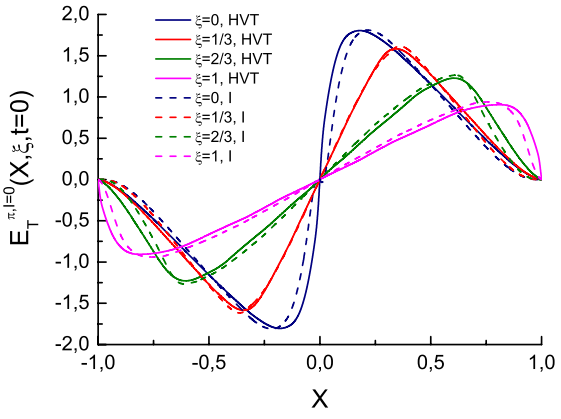

FIG. 9 (color online). The pion tGPD for isoscalar case in the HTV model (solid lines) and in the instanton model (dashed lines) for several values of ξ.

Here, we use the prescription where M^2 in the loop integral is replaced with the combination $M^2 + \Lambda^2$, where in the present context Λ is the cutoff parameter, and then the regularized observable is evaluated according to the formula

$$\mathcal{O}_{\rm reg} = \mathcal{O}(0) - \mathcal{O}(\Lambda^2) + \Lambda^2 d\mathcal{O}(\Lambda^2)/d\Lambda^2. \tag{62}$$

The premultiplying factor $g_\pi^2 = M^2/f_\pi^2$ is not regularized [54,83,84].

In the local model, it is relatively simple to go beyond the chiral limit, hence we do not restrict ourselves to the case $m_\pi = 0$. Since the lattice data used in this work are actually for $m_\pi = 600$ MeV, hence not at all close to the chiral limit of $m = 0$, we need to deal with a situation of moderately large pion masses. The prescription to fix the model parameters is as follows: the three constants Λ, M, and m are traded for the constituent quark mass, M, the pion decay constant f_π, and m_π. We assume that Λ depends on M only, and not on m. Constraining $f_\pi = 93$ MeV (the physical value) and using the given value of m_π leaves us with one free parameter only, M, which is taken in the 250–300 MeV ball park.

We recall that the optimum value of M used in chiral quark models depends of particular observable used for the fitting procedure. The application to the ρ meson suggests M above $m_\rho/2 \sim 400$ MeV, while the soliton models for the nucleon prefer $M \sim 300$–350 MeV [85]. However, significantly lower values follow from other studies in the pion sector. The charge radius of the pion in the NJL model with the Pauli-Villars regulator favors $M \sim 280$ MeV [54], however, the pion-loop corrections to this observable are important. The analysis of the radii of the pion charge and transition form factors from quark triangle diagrams yields $M = \sqrt{2/3}\pi f_\pi \sim 240$ MeV [86]. Another restriction on the value of M follows from the Adler function and the corresponding vacuum polarization contribution to the gyromagnetic factor $g - 2$ of the muon. The loop approach (without and with radiative corrections) [87,88] yields $M = 180$–200 MeV, the analytic perturbation model [89] gives 240 MeV, while the nonlocal chiral quark model [90] suggests 250 MeV. Our chosen value of $\sim$250 MeV falls into this ball park.

In the NJL model, the formulas for the lowest two transversity form factors are very simple,

$$\frac{B^{\pi,u}_{T10}(t)}{m_\pi} = \int_0^1 d\alpha \int_0^{1-\alpha} d\beta K,$$
$$\frac{B^{\pi,u}_{T20}(t)}{m_\pi} = \int_0^1 d\alpha \int_0^{1-\alpha} d\beta \alpha K,$$
$$K = \frac{N_c g_\pi^2 M}{2\pi^2(M^2 + m_\pi^2(\alpha-1)\alpha + t\beta(\alpha+\beta-1))}\Bigg|_{\rm reg}. \tag{63}$$

with $g_\pi = M/f_\pi$. The variables α and β are the Feynman parameters.

The result for the tGPD are particularly simple at $t = 0$ and in the chiral limit, namely, trapezoidal for the symmetric ($I = 1$) combination,

$$E_T^{\pi,S}(X,\xi,t=0;\mu_0)/N = \begin{cases} 1, & 0 \le X \le \xi \\ \frac{1-X}{1-\xi}, & \xi \le X \le 1 \end{cases}, \tag{64}$$

and triangular for the antisymmetric ($I = 0$) combination,

$$E_T^{\pi,A}(X,\xi,t=0;\mu_0)/N = \begin{cases} X/\xi, & 0 \le X \le \xi \\ \frac{1-X}{1-\xi}, & \xi \le X \le 1 \end{cases}. \tag{65}$$

Here, N denotes a normalization constant following from the model.

Other results of the local NJL model, the corresponding plots, and comparisons to the predictions of the nonlocal models will be presented in the following parts, together with the discussion of the QCD evolution.

V. QCD EVOLUTION

We now come to a very important aspect of our analysis. Before comparing the results to the lattice data, we need to carry out the QCD evolution, as the tGPD and tGFFs evolve with the scale. The need for the evolution has been discussed in detail in [43]. In essence, our approach consists of 1) evaluation of the appropriate soft matrix element in the given model at the low quark-model scale, where the matrix element is matched to the QCD result, and 2) subsequent evolution to higher scales with appropriate perturbative QCD equations.

For instance, the lattice data correspond typically to the scale of about $Q = 2$ GeV, as follows from the used value of the lattice spacing, while the quark-model calculation corresponds to a much lower scale,

$$\mu_0 \sim \Lambda_{\rm QCD}. \tag{66}$$

A detailed discussion of the evolution issue and ways to set the quark-model scale is presented in Refs. [43,91], where the scale

$$\mu_0 = 313 \text{ MeV} \tag{67}$$

is advocated. We stress that the inclusion of evolution is crucial for obtaining the results at experimental or lattice scales. A nontrivial test is to check that the procedure reproduces consistently other observables at a given scale, μ (see e.g. Refs. [43,91] for a detailed comparison).

A. Evolution of tGPD

The leading-order DGLAP-ERBL evolution for tGPD is given, e.g., in [6]. To carry out this evolution in practical terms, we use the method given in [92–95], where the basic objects are the moments in the Gegenbauer polynomials of index n

$$g_n(\mu) = \int_0^1 dX E_T^{\pi,S}(X,\xi,t;\mu) G_n^{3/2}(X/\xi). \tag{68}$$

The DGLAP region, $X > \xi$, is outside of the orthogonality range for the polynomials $G_n^{3/2}(X/\xi)$. The LO DGLAP-ERBL evolution amounts to the multiplication

$$g_n(\mu) = L_n g_n(\mu_0), \tag{69}$$

$$L_n = \left(\frac{\alpha(\mu)}{\alpha(\mu_0)}\right)^{\gamma_n^T/(2\beta_0)}. \tag{70}$$

The anomalous dimensions in the transversity (tensor) channel are given by

$$\gamma_n^T = \frac{32}{3} H_n - 8, \tag{71}$$

where $H_n = \sum_{k=1}^n 1/k$. In particular, one has for the two lowest form factors $\gamma_1^T = \frac{8}{3}$ and $\gamma_2^T = 8$. We use $\beta_0 = \frac{11}{3} N_c - \frac{2}{3} N_f$ and the running coupling constant

$$\alpha(\mu) = 4\pi/[\beta_0 \log(\mu^2/\Lambda_{\rm QCD}^2)], \tag{72}$$

with $\Lambda_{\rm QCD} = 226$ MeV for $N_c = N_f = 3$. The inversion of the evolved moments back into the evolved GPD, applied in our calculation, is explained in [92–95].

We also recall that in the transversity channel the quark distributions evolve autonomously, i.e. do not mix with the gluon distributions, which is the case of the vector and axial channels. That way no gluon tGPDs are generated by the QCD evolution, as by construction they vanish in chiral quark models at the quark-model scale.

B. Evolution of transversity form factors

The LO DGLAP-ERBL evolution of tGFFs, defined as moments of the GPDs, has been spelled out explicitly in [14]. The triangular structure which appears from the considerations on the evolution of the tGPDs is, for odd $n = 2k + 1$,

$$B_{2k+1,2l} = k\Gamma(2k) \sum_{m=0}^{k} (4m+3) L_{2m+1} \sum_{j=k-l}^{k} \frac{2^{2(j-k)}(-1)^{m-j}\Gamma(j+m+\frac{3}{2}) B^0_{2j+1,2(j-k+l)}}{\Gamma(2j+1)\Gamma(m-j+1)\Gamma(k-m+1)\Gamma(k+m+\frac{5}{2})}, \tag{73}$$

and, for even $n = 2k + 2$,

$$B_{2k+2,2l} = \Gamma(2k+2) \sum_{m=0}^{k} (4m+5) L_{2m+2} \sum_{j=k-l}^{k} \frac{2^{2j-2k-1}(-1)^{m-j}\Gamma(j+m+\frac{5}{2}) B^0_{2(j+1),2(j-k+l)}}{\Gamma(2j+2)\Gamma(m-j+1)\Gamma(k-m+1)\Gamma(k+m+\frac{7}{2})}, \tag{74}$$

where $k = 0, 1, 2, \ldots$ and $l = 0, 1, \ldots, k$. We have introduced a shorthand notation $B_{ni} = B_{Tni}^{\pi}(t;\mu)$ and $B_{ni}^0 = B_{Tni}^{\pi}(t;\mu_0)$. For the lowest moments we have, explicitly,

$$\begin{aligned}
B_{10} &= L_1 B_{10}^0, \\
B_{32} &= \frac{1}{5}(L_1 - L_3) B_{10}^0 + L_3 B_{32}^0, \\
B_{54} &= \frac{1}{105}(9L_1 - 14L_3 + 5L_5) B_{10}^0 + \frac{2}{3}(L_3 - L_5) B_{32}^0 \\
&\quad + L_5 B_{54}^0, \\
&\ldots \\
B_{20} &= L_2 B_{20}^0, \\
B_{42} &= \frac{3}{7}(L_2 - L_4) B_{20}^0 + L_4 B_{42}^0, \\
&\ldots \\
B_{30} &= L_3 B_{30}^0, \\
B_{52} &= \frac{2}{3}(L_3 - L_5) B_{30}^0 + L_5 B_{52}^0, \\
&\ldots \\
B_{40} &= L_4 B_{40}^0.
\end{aligned} \tag{75}$$

In particular, the two lowest tGFFs available from the lattice data, $B_{T10}^{\pi,u}$ and $B_{T20}^{\pi,u}$, evolve multiplicatively as follows:

$$B_{Tn0}^{\pi,u}(t;\mu) = B_{Tn0}^{\pi,u}(t;\mu_0)\left(\frac{\alpha(\mu)}{\alpha(\mu_0)}\right)^{\gamma_n^T/(2\beta_0)},$$

which numerically gives

$$\begin{aligned}
B_{T10}^{\pi,u}(t;2\ {\rm GeV}) &= 0.75 B_{T10}^{\pi,u}(t;\mu_0), \\
B_{T20}^{\pi,u}(t;2\ {\rm GeV}) &= 0.43 B_{T20}^{\pi,u}(t;\mu_0).
\end{aligned} \tag{76}$$

Note a stronger reduction for B_{T20} compared to B_{T10} as the result of the evolution.

In the chiral limit and at $t = 0$

$$B_{T10}^{\pi,u}(t=0;\mu_0)/m_\pi = \frac{N_c M}{4\pi^2 f_\pi^2}, \tag{77}$$

$$\frac{B_{T20}^{\pi,u}(t=0;\mu)}{B_{T10}^{\pi,u}(t=0;\mu)} = \frac{1}{3}\left(\frac{\alpha(\mu)}{\alpha(\mu_0)}\right)^{8/27}. \tag{78}$$

VI. NUMERICAL RESULTS AFTER THE QCD EVOLUTION

In this section, we present our numerical results *after the QCD evolution* for the tGPD of the pion, its special cases $\xi = 0$ and $\xi = 1$, corresponding to the tPDF and tDA, respectively, as well as discuss the tGFFs. The latter are compared to the available lattice data of [17].

A. tGPD

The results of the calculation of the tGPD of the pion at a sample value of $\xi = 1/3$ and at $t = 0$, together with the LO DGLAP-ERBL evolution, are given in Figs. 10 and 11. For the nonlocal case, we take the HTV model (43) and (50), as the results of the instanton model (42) and (49) are qualitatively similar. Here, we take for simplicity the chiral limit, $m_\pi = 0$. We provide in the figures the symmetric (S) and asymmetric (A) combinations in the X variable (25). The solid lines correspond to the calculation at the quark-model scale, μ_0. In this case we conventionally normalize the plotted functions with a constant N in such a way that

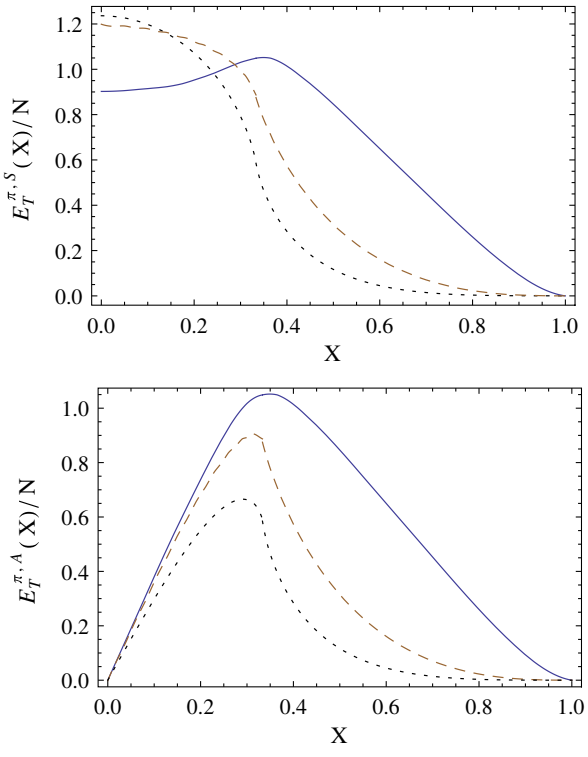

FIG. 10 (color online). The DGLAP-ERBL evolution of the symmetric (S, or $I = 1$) and antisymmetric (A, or $I = 0$) parts of the quark tGPD of the pion in the nonlocal HTV model for $m_\pi = 0$, $t = 0$, $\xi = 1/3$, and $M = 240$ MeV. The solid line corresponds to the initial condition at the quark-model scale $\mu_0 = 313$ MeV, the dashed line shows the result of the evolution to $\mu = 2$ GeV, and the dotted line to $\mu = 1$ TeV.

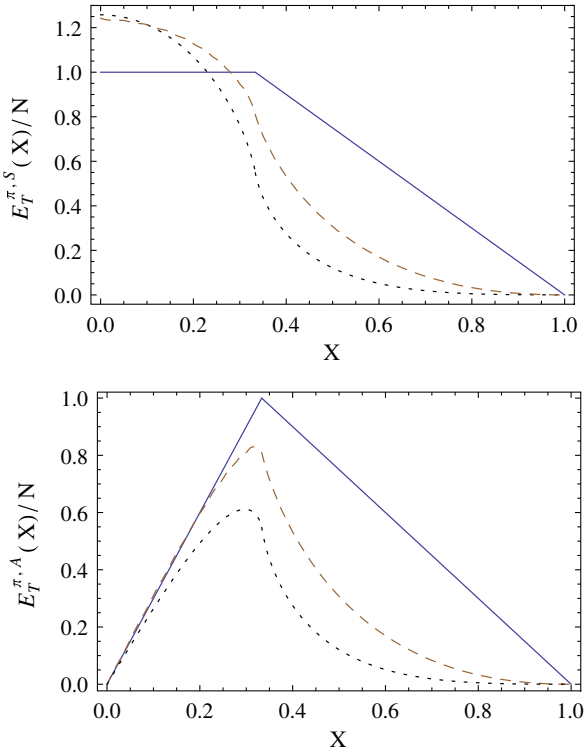

FIG. 11 (color online). (Color online) Same as Fig. 10 for the local NJL model.

$$\int_0^1 dX E_T^{\pi,S}(X, \xi, t = 0; \mu_0)/N = \frac{1+\xi}{2} \qquad (79)$$

for all displayed models.

Further, we note the gross qualitative similarity between the nonlocal HTV model and the local NJL model. The differences are manifest in the end point behavior. Near $X = 1$ the tGPD in nonlocal model is suppressed, as explained in Sec. IVA. Also, near $X = 0$ the quantity $E_T^{\pi,S}$ is depleted compared to the local case, where no minimum is present.

The dashed and dotted curves show the results evolved to the scales 2 GeV and 1 TeV, respectively. After the evolution, the results of the HTV model and the local NJL model are qualitatively very similar.

B. tPDF

Next, we explore the special case $\xi = 0$, again for $t = 0$ and $m_\pi = 0$. In this case tGPD corresponds, by definition, to tPDF. In Fig. 12, we compare the predictions of the three considered models at the quark-model scale, μ_0. We note different end point behavior, both at $X = 1$ and at $X = 0$, according to the discussion presented in Sec. IVA. Near $X = 1$, the instanton model has a stronger suppression in tPDF than the HTV model. The local model approaches zero linearly. Again, we note that the QCD evolution changes the end point behavior.

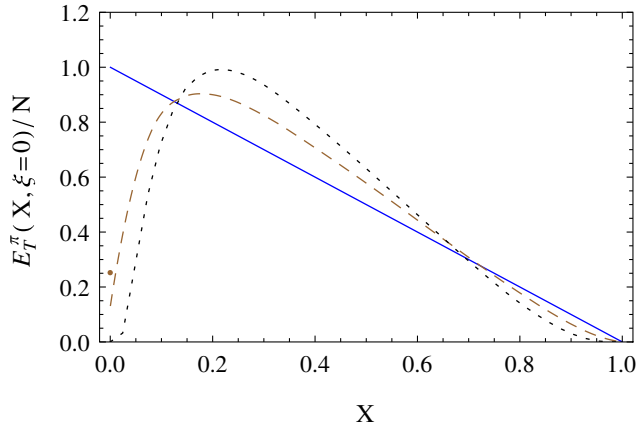

FIG. 12 (color online). (Color online) Comparison of the tPDF ($E_T^\pi(X, t = 0, \xi = 0)$) in the local model (solid line), instanton model (dashed line), and the HTV model (dotted line) for $m_\pi = 0$, evaluated at the quark-model scale.

C. tDA

Another interesting limiting case is provided with $\xi = 1$. In that case

$$E_T^\pi(X, t = 0, \xi = 1) = \phi_T(X), \tag{80}$$

where $\phi_T^\pi(X)$ is the tensor distribution amplitude of the pion, defined as

$$\langle 0|\bar{d}(z)\sigma_{\alpha\beta}\gamma_5 u(-z)|\pi^+(q)\rangle = i\frac{\sqrt{2}}{3}N^T(p_\alpha z_\beta - p_\beta z_\alpha) \times \int_0^1 du e^{i(2u-1)q\cdot z}\phi_T^\pi(u), \tag{81}$$

where $X = 2u - 1$ and N^T is the normalization factor yielding $\int_0^1 du\phi_T(u) = 1$.

The local NJL model predicts a constant $\phi_T^\pi(X)$ at the quark-model scale. Again, as seen from Fig. 13, the difference between the local and nonlocal models is seen in the end point behavior, $X \sim \pm 1$. In the intermediate range of X the tDA $\phi_T^\pi(X)$ is close to a constant also for the nonlocal models.

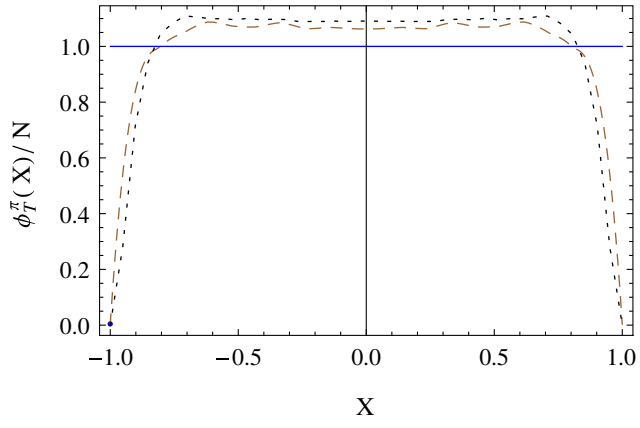

FIG. 13 (color online). (Color online) Comparison of the tDA ($\phi_T^\pi(X)$) in the local model (solid line), instanton model (dashed line), and the HTV model (dotted line) for $m_\pi = 0$, evaluated at the quark-model scale.

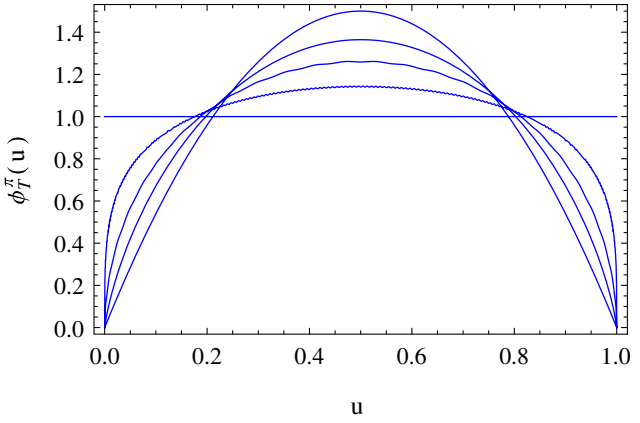

FIG. 14 (color online). (Color online) Evolution of the tensor distribution amplitude, tDA, in the local NJL model. The subsequent curves (from bottom to top at $u = 1/2$) correspond to $\mu = \mu_0 = 313$ MeV (the constant), $\mu = 500$ MeV, $\mu = 2$ GeV, $\mu = 1000$ GeV, and $\mu = \infty$ (the asymptotic form $6u(1 - u)$).

In Fig. 14, we show the LO ERBL evolution of the tDA of the pion in the local NJL model. We note a gradual approach toward the asymptotic form

$$\phi_{T,\text{asym}}^\pi(u) = 6u(1 - u). \tag{82}$$

For the nonlocal models, the effect of the evolution is similar.

D. tGFFs

In Fig. 15, we show the LO DGLAP-ERBL evolution of the tGFFs evaluated in the local NJL model.

By comparing the two panels of Fig. 15, we note that the evolution of tGFFs is multiplicative, and increasing the scale leads to quenching of the form factors B_{Tn0}. For the form factors B_{Tni} with $i \neq 0$ the evolution is more complicated, as can be inferred from Eq. (75). For the nonlocal models, the effects of the evolution for tGFFs are similar.

E. Chiral quark models vs lattice

The content of this section has already been presented by us in a greater detail in [19]. For the completeness of the present work, we repeat the main results.

The presently available full-QCD lattice results [17] are for $B_{10}^{\pi,u}$ and $B_{20}^{\pi,u}$ and for $-t$ up to 2.5 GeV^2, with moderately low, but still away from the physical limit, values of the pion mass, $m_\pi \sim 600$ MeV. The calculation of [17] uses the same $N_f = 2$ set of the QCDSF/UKQCD ensembles with improved Wilson fermions and the Wilson gauge action that were used previously in the analysis of the pion charge and gravitational form factors [96].

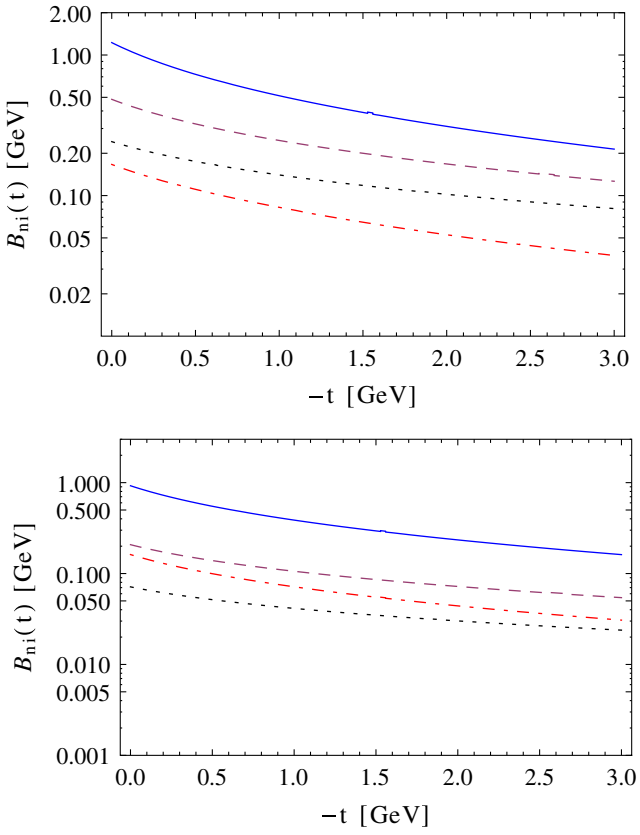

FIG. 15 (color online). (Color online) The transversity form factors $B^u_{ni}(t)$, evaluated in the local NJL model at the quark-model scale μ_0 (top panel) and evolved to $\mu = 2$ GeV (bottom panel). Solid line—$B^u_{10}(t)$, dashed line—$B^u_{20}(t)$, dotted line—$B^u_{30}(t)$, dash-dotted line—$B^u_{32}(t)$.

We note that for $t = 0$, both the local and nonlocal models yield the normalization

$$B^{\pi,u}_{T10}(t=0;\mu_0)/m_\pi = \frac{N_c}{2\pi^2 f_\pi^2}\int_0^\infty du\,\frac{um^2(u)}{(u+m^2(u))^3}(m(u)-um'(u)), \tag{83}$$

$$B^{\pi,u}_{T20}(t=0;\mu_0)/m_\pi = \frac{N_c}{2\pi^2 f_\pi^2}\left\{\int_0^\infty du\,\frac{um(u)}{(u+m^2(u))^3}(m^2(u) + \frac{1}{2}um(u)m'(u) + \frac{1}{6}u^2m'^2(u)) - \int_0^\infty du\,\frac{u^2m^2(u)}{(u+m^2(u))^4}(m(u)+2m^2(u)m'(u))\right\}, \tag{84}$$

where $m'(u) = dm(u)/du$. In the local limit, where $m(k^2) \to$ const, one reproduces Eqs. (77) and (78).

The results for $B^{\pi,u}_{Tn0}(t)$, $n = 1, 2$, are shown in Fig. 16. In our study, we have assumed that B_{Tn0}/m_π depends weakly on m_π, similarly to the local model case [19]. Therefore, to compare to the lattice data for B_{Tn0}, we multiply the results of the calculations obtained in the chiral limit with $m_\pi = 600$ MeV. We have carried out the QCD evolution procedure as described in the previous Sections, from the quark-model scale up to the lattice scale of 2 GeV. From Fig. 16 we note that the HTV model with the vertex function given by Eq. (43) (solid lines) and with $M_q = 300$ MeV works best, describing accurately the data, while the instanton model, Eq. (42) (dashed lines), results in form factors falling-off too steeply. We have found that lower values of M_q spoil the agreement with the lattice data.

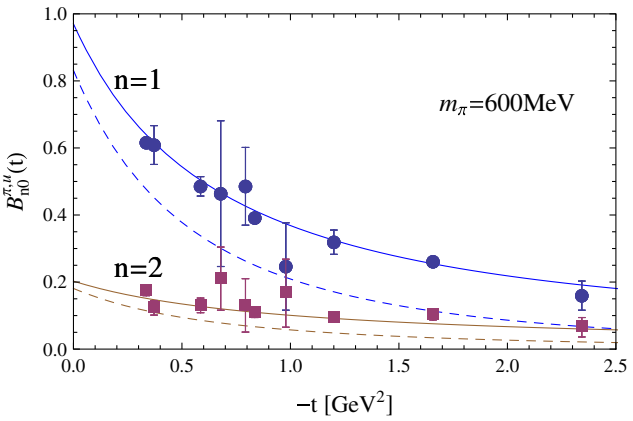

FIG. 16 (color online). (Color online) The transversity form factors in the HTV model (solid line) and in the instanton model (dashed line). The data come from [96].

In Fig. 17, we show the results from the local NJL model evolved to the lattice scale of $\mu = 2$ GeV, confronted with the lattice data scanned from Fig. 1 of [17]. We have used $m_\pi = 600$ MeV and selected $M = 250$ MeV, which optimizes the comparison. As we see, the agreement is remarkable.

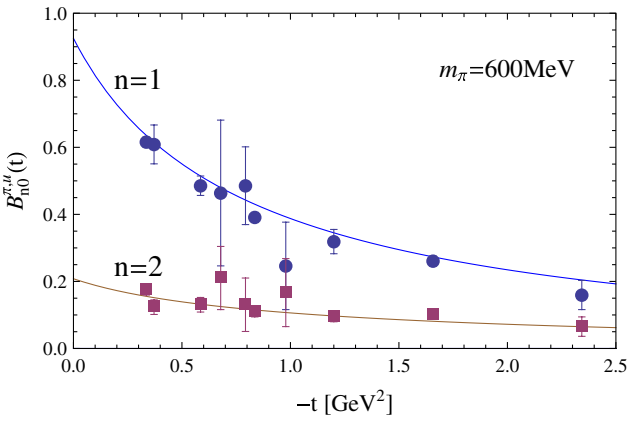

FIG. 17 (color online). (Color online) The transversity form factors obtained in the NJL model (lines) for $M = 250$ MeV and $m_\pi = 600$ MeV, evolved to the lattice scale of 2 GeV and compared to the lattice data from Fig. 1 of [17] (points).

In Ref. [19], we have also investigated the dependence of the values of the form factors at $t = 0$ on the value of m_π, as studied in [17]. We have also noted in [19] that the results presented in Fig. 17 depend quite sensitively on the value of the constituent quark mass, M, with higher M yielding lower values of the transversity form factors.

VII. CONCLUSIONS

In the present paper, we have shown how the spinless pion acquires a nontrivial spin structure within the framework of chiral quark models. This has been achieved by computing the transversity distributions, corresponding to matrix elements of the tensor quark density, within chiral quark models, where the pion arises as the pseudo-Goldstone boson of the spontaneously broken chiral symmetry. Moreover, we have worked at the leading order in the $1/N_c$ expansion, which amounts to carrying out one-quark-loop calculations, where the implementation of the symmetry constraints becomes absolutely essential. Chiral symmetry is respected by implementing the pertinent chiral Ward-Takahashi identities at the quark level. Moreover, the relativity constraints are fulfilled in terms of the polynomiality conditions which are manifestly preserved through the use of the double distributions, or, equivalently, by working with the α-representations.

We have provided comprehensive results for the tGPDs of the pion, as well as related quantities following from restrained kinematics, evaluation of moments, or taking the Fourier-Bessel transforms to the impact-parameter space. We have also shown in detail various technical aspects of our analysis, including the use of the α-representation in the nonlocal models.

The generated tGPDs are defined at a given low-energy quark-model scale, and comparison to data or lattice results corresponds to implementing the suitable QCD evolution. Actually, while the momentum-transfer or, equivalently, the impact-parameter dependence of the tGFFs remains scale independent, their absolute normalization does depend multiplicatively on the renormalization scale. Remarkably, the absolute predictions for the multiplicatively evolved B_{Tn0}, for $n = 1, 2$, agree surprisingly well with the lattice results, supporting many previous calculations following the same chiral-quark-model scheme amended with the subsequent QCD evolution.

ACKNOWLEDGMENTS

One of us (A. E. Dorokhov) is thankful to A. V. Radyushkin and S. V. Mikhailov for numerous discussions. Supported by the Bogoliubov-Infeld program (JINR), the Polish Ministry of Science and Higher Education, Grants No. N N202 263438 and No. N N202 249235, Spanish DGI and FEDER Grant No. FIS2008-01143/FIS, Junta de Andalucía Grant No. FQM225-05, and EU Integrated Infrastructure Initiative Hadron Physics Project, Contract No. RII3-CT-2004-506078. A. E. D. acknowledges partial support from the Russian Foundation for Basic Research, Projects No. 10-02-00368 and No. 11-02-00112.

[1] C. G. Callan, Jr. and D. J. Gross, Phys. Rev. Lett. **22**, 156 (1969).
[2] V. Barone, A. Drago, and P. G. Ratcliffe, Phys. Rep. **359**, 1 (2002).
[3] D. Mueller, D. Robaschik, B. Geyer, F. M. Dittes, and J. Horejsi, Fortschr. Phys. **42**, 101 (1994).
[4] X.-D. Ji, Phys. Rev. Lett. **78**, 610 (1997).
[5] A. V. Radyushkin, Phys. Lett. B **380**, 417 (1996).
[6] A. V. Belitsky and A. V. Radyushkin, Phys. Rep. **418**, 1 (2005).
[7] T. Feldmann, Eur. Phys. J. Special Topics **140**, 135 (2007).
[8] S. Boffi and B. Pasquini, Riv. Nuovo Cimento Soc. Ital. Fis. **30**, 387 (2007).
[9] M. Burkardt, Phys. Rev. D **62**, 071503 (2000).
[10] M. Burkardt, Int. J. Mod. Phys. A **18**, 173 (2003).
[11] M. Burkardt and S. Dalley, Prog. Part. Nucl. Phys. **48**, 317 (2002).
[12] B. U. Musch, P. Hagler, J. W. Negele, and A. Schafer, Phys. Rev. D **83**, 094507 (2011).
[13] P. Hagler, Phys. Rep. **490**, 49 (2010).
[14] W. Broniowski and E. R. Arriola, Phys. Rev. D **79**, 057501 (2009).
[15] M. Diehl and P. Hagler, Eur. Phys. J. C **44**, 87 (2005).
[16] M. Burkardt, Phys. Rev. D **72**, 094020 (2005).
[17] D. Brommel *et al.* (QCDSF), Phys. Rev. Lett. **101**, 122001 (2008).
[18] M. Diehl and L. Szymanowski, Phys. Lett. B **690**, 149 (2010).
[19] W. Broniowski, A. E. Dorokhov, and E. R. Arriola, Phys. Rev. D **82**, 094001 (2010).
[20] S.-i. Nam and H.-C. Kim, Phys. Lett. B **700**, 305 (2011).
[21] X.-D. Ji, J. Phys. G **24**, 1181 (1998).
[22] A. V. Radyushkin, in *At the frontier of particle physics. Handbook of QCD*, edited by M. Shifman (World Scientific, Singapore, 2002).
[23] K. Goeke, M. V. Polyakov, and M. Vanderhaeghen, Prog. Part. Nucl. Phys. **47**, 401 (2001).
[24] A. P. Bakulev, R. Ruskov, K. Goeke, and N. G. Stefanis, Phys. Rev. D **62**, 054018 (2000).
[25] M. Diehl, Phys. Rep. **388**, 41 (2003).
[26] X.-D. Ji, Annu. Rev. Nucl. Part. Sci. **54**, 413 (2004).
[27] R. M. Davidson and E. Ruiz Arriola, Phys. Lett. B **348**, 163 (1995).
[28] E. Ruiz Arriola, in *Proc. of the workshop Lepton Scattering, Hadrons and QCD, Adelaide, Australia,*

2001, edited by W. Melnitchouk *et al.* (World Scientific, Singapore, 2001).
[29] R. M. Davidson and E. Ruiz Arriola, Acta Phys. Pol. B **33**, 1791 (2002).
[30] W. Broniowski and E. Ruiz Arriola, Phys. Lett. B **574**, 57 (2003).
[31] A. E. Dorokhov and L. Tomio, arXiv:hep-ph/9803329.
[32] M. V. Polyakov and C. Weiss, Phys. Rev. D **60**, 114017 (1999).
[33] A. E. Dorokhov and L. Tomio, Phys. Rev. D **62**, 014016 (2000).
[34] I. V. Anikin, A. E. Dorokhov, A. E. Maksimov, L. Tomio, and V. Vento, Nucl. Phys. **A678**, 175 (2000).
[35] M. Praszalowicz and A. Rostworowski, in *Proc. of the XXXVIIth Rencontres de Moriond, Les Arcs, France* (2002).
[36] M. Praszalowicz and A. Rostworowski, Acta Phys. Pol. B **34**, 2699 (2003).
[37] A. Bzdak and M. Praszalowicz, Acta Phys. Pol. B **34**, 3401 (2003).
[38] R. J. Holt and C. D. Roberts, Rev. Mod. Phys. **82**, 2991 (2010).
[39] T. Nguyen, A. Bashir, C. D. Roberts, and P. C. Tandy, Phys. Rev. C **83**, 062201 (2011).
[40] L. Theussl, S. Noguera, and V. Vento, Eur. Phys. J. A **20**, 483 (2004).
[41] F. Bissey, J. R. Cudell, J. Cugnon, J. P. Lansberg, and P. Stassart, Phys. Lett. B **587**, 189 (2004).
[42] S. Noguera and V. Vento, Eur. Phys. J. A **28**, 227 (2006).
[43] W. Broniowski, E. Ruiz Arriola, and K. Golec-Biernat, Phys. Rev. D **77**, 034023 (2008).
[44] T. Frederico, E. Pace, B. Pasquini, and G. Salme, Nucl. Phys. B, Proc. Suppl. **199**, 264 (2010).
[45] T. Frederico, E. Pace, B. Pasquini, and G. Salme, Phys. Rev. D **80**, 054021 (2009).
[46] M. V. Polyakov, Nucl. Phys. **B555**, 231 (1999).
[47] S. V. Esaibegian and S. N. Tamarian, Sov. J. Nucl. Phys. **51**, 310 (1990).
[48] A. E. Dorokhov, Nuovo Cimento Soc. Ital. Fis. A **109**, 391 (1996).
[49] V. Y. Petrov, M. V. Polyakov, R. Ruskov, C. Weiss, and K. Goeke, Phys. Rev. D **59**, 114018 (1999).
[50] I. V. Anikin, A. E. Dorokhov, and L. Tomio, Phys. Lett. B **475**, 361 (2000).
[51] M. Praszalowicz and A. Rostworowski, Phys. Rev. D **64**, 074003 (2001).
[52] A. E. Dorokhov, JETP Lett. **77**, 63 (2003).
[53] E. Ruiz Arriola and W. Broniowski, Phys. Rev. D **66**, 094016 (2002).
[54] E. Ruiz Arriola, Acta Phys. Pol. B **33**, 4443 (2002).
[55] W. Broniowski and E. Ruiz Arriola, Phys. Rev. D **78**, 094011 (2008).
[56] B. Pire and L. Szymanowski, Phys. Rev. D **71**, 111501 (2005).
[57] B. Pire and L. Szymanowski, Phys. Lett. B **622**, 83 (2005).
[58] J. P. Lansberg, B. Pire, and L. Szymanowski, Phys. Rev. D **73**, 074014 (2006).
[59] J. P. Lansberg, B. Pire, and L. Szymanowski, in *proc. of Exclusive Reactions at High Momentum Transfer, Jefferson Lab, 2007*, edited by A. Radyushkin and P. Stoler (World Scientific eBooks, 2007).
[60] B. C. Tiburzi, Phys. Rev. D **72**, 094001 (2005).
[61] W. Broniowski and E. Ruiz Arriola, Phys. Lett. B **649**, 49 (2007).
[62] A. Courtoy and S. Noguera, Phys. Rev. D **76**, 094026 (2007).
[63] A. Courtoy and S. Noguera, Prog. Part. Nucl. Phys. **61**, 170 (2008).
[64] P. Kotko and M. Praszalowicz, Acta Phys. Pol. B **40**, 123 (2009).
[65] P. J. Sutton, A. D. Martin, R. G. Roberts, and W. J. Stirling, Phys. Rev. D **45**, 2349 (1992).
[66] M. Gluck, E. Reya, and I. Schienbein, Eur. Phys. J. C **10**, 313 (1999).
[67] C. Best *et al.*, Phys. Rev. D **56**, 2743 (1997).
[68] D. Diakonov and V. Y. Petrov, Nucl. Phys. **B272**, 457 (1986).
[69] B. Holdom, J. Terning, and K. Verbeek, Phys. Lett. B **245**, 612 (1990).
[70] P. Maris, C. D. Roberts, and P. C. Tandy, Phys. Lett. B **420**, 267 (1998).
[71] N. Bogolyubov and D. Shirkov *Introduction to the Theory of Quantized Fields* (Wiley, New York, 1980).
[72] O. Zavialov *Renormalized Quantum Field Theory*(Kluwer Academic, Dordrecht, 1990).
[73] A. V. Radyushkin, Phys. Rev. D **56**, 5524 (1997).
[74] A. E. Dorokhov, arXiv:1003.4693.
[75] A. E. Dorokhov, JETP Lett. **92**, 707 (2010).
[76] A. V. Radyushkin, Phys. Rev. D **83**, 076006 (2011).
[77] W. Broniowski, E. Ruiz Arriola, and K. Golec-Biernat, Phys. Rev. D **77**, 034023 (2008).
[78] I. A. Perevalova, M. V. Polyakov, A. N. Vall, and A. A. Vladimirov arXiv:1105.4990.
[79] V. Gribov, arXiv:hep-ph/0006158.
[80] J. Gasser and H. Leutwyler, Ann. Phys. (N.Y.) **158**, 142 (1984).
[81] W. Broniowski, arXiv:hep-ph/9911204.
[82] H. Pagels and S. Stokar, Phys. Rev. D **20**, 2947 (1979).
[83] E. Ruiz Arriola, Phys. Lett. B **253**, 430 (1991).
[84] C. Schuren, E. Ruiz Arriola, and K. Goeke, Nucl. Phys. **A547**, 612 (1992).
[85] C. V. Christov *et al.*, Prog. Part. Nucl. Phys. **37**, 91 (1996).
[86] S. B. Gerasimov, Yad. Fiz. **29**, 513 (1979).
[87] A. A. Pivovarov, Phys. At. Nucl. **66**, 902 (2003).
[88] R. Boughezal and K. Melnikov, arXiv:1104.4510.
[89] K. A. Milton, I. L. Solovtsov, and O. P. Solovtsova, Phys. Rev. D **64**, 016005 (2001).
[90] A. E. Dorokhov, Phys. Rev. D **70**, 094011 (2004).
[91] W. Broniowski and E. Ruiz Arriola, Phys. Rev. D **79**, 057501 (2009).
[92] N. Kivel and L. Mankiewicz, Phys. Lett. B **458**, 338 (1999).
[93] N. Kivel and L. Mankiewicz, Nucl. Phys. **B557**, 271 (1999).
[94] A. Manashov, M. Kirch, and A. Schafer, Phys. Rev. Lett. **95**, 012002 (2005).
[95] M. Kirch, A. Manashov, and A. Schafer, Phys. Rev. D **72**, 114006 (2005).
[96] D. Brommel *et al.*, Proc. Sci., LAT2005 (2006) 360.